X-ray diffraction and theoretical study of the transition 2H-3R polytypes in $Nb_{1+x}Se_2$ (0 < x <0.1)

Mohamed Sidoumou [1], **Soumia Merazka** [2], **Adrian Gómez-Herrero** [3], **Mohammed Kars** [Corresp., 2], **Roisnel Thierry** [4]

[1] Département de Physique, Laboratoire de physique théorique et interaction rayonnement matière, Université de Blida-1, Soumaa Blida, Algérie

[2] Faculté de Chimie, Laboratoire Sciences des matériaux, Université Houari-Boumedienne, Algérie., El-Alia Bab-Ezzouar, Algérie

[3] Centro de Microscopia Electrónica, Universidad Complutense de Madrid, Madrid, Spain

[4] CNRS, ISCR (Institut des Sciences Chimiques de Rennes), Université de Rennes 1, Rennes, France

Corresponding Author: Mohammed Kars
Email address: mkarsdz@yahoo.fr

Single crystals of 2H and 3*R* niobium diselenide were grown by a chemical transport reaction. The current determinations by single crystals X-ray diffraction reveal a non-stoichiometric composition. The structures are built from Se—Nb—Se slabs with Nb in trigonal prismatic coordination whereas the extra or additional Nb atoms are located in the octahedral holes between the slabs giving rise to the formula 2H and 3*R*-$Nb_{1+x}Se_2$ with 0.07< x <0.118. In particular, vacancy and Nb-Nb interactions may play an important role on the non-stoichiometry and the stacking mode in $NbSe_2$. By increasing the number of additional Nb atoms in the pure 2H-$NbSe_2$, a transition 2H to 3R polytype should occur in order to minimize the Nb_{layer}—Nb_{extra}—Nb_{layer} repulsions between these adjacent slabs. The theoretical study shows that both 2H and 3R-$Nb_{1+x}Se_2$ are thermodynamically stable in the range 0< x <0.1.

X-ray diffraction and theoretical study of the transition 2H-3R polytypes in $Nb_{1+x}Se_2$ (0< x <0.1)

Mohamed Sidoumo[1], Soumia Merazka[2], Adrian Gómez-Herrero[3], Mohammed Kars[2]*, Thierry Roisnel[4]

[1] Département de Physique, Laboratoire de physique théorique et interaction rayonnement matière, Université Blida1, Soumaa Blida, Algérie.

[2] Faculté de Chimie, Laboratoire Sciences des matériaux, Université des Sciences et de la Technologie Houari-Boumediene, El-Alia Bab-Ezzouar, Algérie.

[3] Centro de Microscopia Electrónica, Universidad Complutense, Madrid, Spain.

[4] CNRS, ISCR (Institut des Sciences Chimiques de Rennes), Université de Rennes 1, Rennes, France.

Corresponding Author:

Mohammed Kars

Faculté de Chimie, Laboratoire Sciences des matériaux, Université des Sciences et de la Technologie Houari-Boumediene, El-Alia Bab-Ezzouar, Algérie.

Email address: mkarsdz@yahoo.fr

36

Abstract

38   Single crystals of 2H and 3R niobium diselenide were grown by a chemical transport reaction.

39   The current determinations by single crystals X-ray diffraction reveal a non-stoichiometric

40   composition. The structures are built from Se—Nb—Se slabs with Nb in trigonal prismatic

41   coordination whereas the extra or additional Nb atoms are located in the octahedral holes

42   between the slabs giving rise to the formula 2H and 3R-Nb$_{1+x}$Se$_2$ with 0.07< x <0.118. In

43   particular, vacancy and Nb-Nb interactions may play an important role on the non-stoichiometry

44   and the stacking mode in NbSe$_2$. By increasing the number of additional Nb atoms in the pure

45   2H-NbSe$_2$, a transition 2H to 3R polytype should occur in order to minimize the Nb_{layer}—

46   Nb_{extra}—Nb_{layer} repulsions between these adjacent slabs.

47   The theoretical study shows that both 2H and 3R-Nb$_{1+x}$Se$_2$ are thermodynamically stable in the

48   range 0< x <0.1.

49
50

Introduction

52   NbSe$_2$ belongs to the transition metal dichalcogenides TMDC's with chemical formula TX$_2$ (T =

53   Nb, Ta; X = S, Se), which have recently renewed interest because of their quasi 2D nature

54   similar to graphene making them very promising in novel electronic devices applications (Vogel

55   & Robinson, 2015). The system NbSe$_2$ has been the subject of many investigations since it

56   exhibits incommensurate charge density waves (CDW) and superconductivity phenomenon

57   above 4K (Wilson, Disalvo & Mahajan, 1975).

58   The structure consists in hexagonally arranged Se-Nb-Se sandwiches with metal atoms (Nb)

59   that are located between two layers of chalcogen atoms (Se) in a trigonal prismatic coordination.

60   The bonding within each sandwich is covalent while the bonding among sandwiches themselves

61   is a weak Van-der Waals type. Although the stacking along the c axis gives rise to several

62   polytypes usually described as 1T–NbSe$_2$, 2H- NbSe$_2$, 3R– NbSe$_2$ and 4H- NbSe$_2$ (Kalikhman &

63   Umanskii, 1973; Brown & Beerntsen, 1965), it seems that only the 2H and 3R are frequently

64   obtained in practice.

65   Until date, there are many reports on polymorphism in the TMDC's by tuning synthesis

66   temperature such as the high temperature monoclinic MoTe$_2$ (Brown, 1966), the layered telluride

67   Mo$_{1-x}$Nb$_x$Te$_2$ (Ikeura et al., 2015), polytypism in TiS$_2$ which was first observed by Tronc et al.,

68 (1973) and Legendre et al. (1975), the highly polymorphic $TaSe_2$ (Brown & Beerntsen, 1965;

69 Huisman, Kadijk & Jellinek, 1970) and the polymorph $TaSe_{2-x}Te_x$ (Luo et al., 2015).

70 This structural anisotropy enables the intercalation of species to form stoichiometric and non-

71 stoichiometric compounds with different guests. A number of authors (Huisman, Kadijk &

72 Jellinek, 1970 and references therein) reported the existence of the Nb self-intercalation (SI) in

73 $NbSe_2$ phases where the additional Nb metal atoms lie in octahedral holes between $NbSe_2$ layers.

74 Most of the structures were characterized by X-ray powder diffraction method, and very few

75 investigations using single crystal X-ray diffraction technique were performed.

76 The Nb-Se phase diagram has been established on the basis of the homogeneity range of several

77 polytypes which mostly depend on the method and the synthesis conditions (Predel, 1997).

78 However, and according to the recent findings (Ivanova et al., 2019), the diagram may contain

79 some ambiguous data and should be revisited

80 The selenide $2H-NbSe_2$ revisited by single crystals (Meerschaut & Deudon, 2001) and the

81 selenide $3R-NbSe_2$ investigated on the basis of the precession photograph (Huisman, Kadijk &

82 Jellinek, 1970) have been both found stoichiometric; while the sulfur polytype $3R-Nb_{1+x}S_2$ ($x =$

83 0.06 and 0.09) (Meerschaut & Deudon, 2001., Powell & Jacobson, 1981) is non-stoichiometric.

84 According to Fisher and Sienko (1980), these compounds are non-stoichiometric. Indeed, in the

85 $2H-NbSe_2$, the niobium atoms are stacked directly one above the other along the c axis, which is

86 not the case for $3R-NbSe_2$. In the case of an excessive intercalate niobium a transition from 2H to

87 3R polytype should then occur in order to minimize the $Nb_{layer}—Nb_{extra}—Nb_{extra}$ repulsions

88 between these adjacent slabs. This transition was explained by an NbS_2-layers rotation

89 mechanism involving stacking faults probabilities between 15-18% (Katzke, 2002; Leroux et al.,

90 2018).

91 In this work, three polytypes in the Nb-Se system: $2H-Nb_{1.031}Se_2$, $3R-Nb_{1.071}Se_2$ and $3R-$

92 $Nb_{1.085}Se_2$ were synthesized by CVT and investigated by single crystal X-ray diffraction.

93 In particular, the role of vacancy and Nb-Nb interactions on the non-stoichiometry and stacking

94 mode in $NbSe_2$ has been examined.

95 Both 2H and 3R polytypes may co-exist in the range 0< x <0.07 and above this limit where only

96 the form 3R predominates as a transition 2H-3R will take place.

97   Furthermore, by using DFT with CASTEP code, a comparative study involving thermodynamic

98   polytype stability of 2H and 3R-$Nb_{1+x}Se_2$ (x = 0, 0.1) has been attempted in order to support the

99   X-ray diffraction conclusions.

100

101

102   **Materials & Methods**

103

104   **Crystal growth and chemical analysis**

105   Single crystals of 2H and 3R-$Nb_{1+x}Se_2$ were obtained by chemical vapor transport (CVT) method

106   during our attempts to prepare ternary $HgNbSe_2$ and $SnNbSe_2$. A stoichiometric amount of pure

107   elements with an excess of Se were mixed and sealed in an evacuated quartz tube (length ~ 18

108   cm) using iodine (<5 mg/cm^3) as a transport agent to favour crystallization. The mixtures (charge

109   ~ 1g) were placed into a zone tube furnace. The temperature was first increased slowly at 500 °C

110   and held then for 48h in order to avoid thermal runaway caused by the exothermic reaction

111   between Nb and Se. After that the temperature is turned up between 760-1050 °C for 15 days.

112   Finally the furnace was allowed to cool slowly to room temperature. Crystals of appreciable

113   sizes were grown in the cold end of the tube; 2H+3R crystals are obtained at ~ 760 °C while the

114   3R crystals are obtained at ~ 1050°C. The analysis results by X-ray energy dispersive

115   spectroscopy (XEDS) with the TEM (EDX Oxford Instruments) on several different crystallites

116   of each polytype sample gave an approximate atomic ratio of 1:2 for Nb and Se [for a selected

117   3R-crystal: Nb (at%) = 29,9 and Se (at%) = 70,1].

118

119   **Single crystal structure determination**

120   Single crystals data were recorded on a Kappa Apex II CCD X-ray diffractometer (Bruker AXS

121   2006) with graphite-monochromated MoKα (λ = 0.71071 Å) radiation. The reflection intensities

122   were integrated with the SAINT (Bruker APEX2, 2006); SADABS was used for empirical

123   absorption correction (Sheldrick , 2002), and Jana 2006 (Petříček et al., 2006) was performed for

124   the structure refinement.

125   The crystal structure of 3R-$Nb_{1.071}Se_2$ was obverse/reverse twinned while the 3R-$Nb_{1.085}Se_2$ was

126   twinned by inversion; with a refined twin domain fraction of 0.611(5) : 0.389(5) and 0.85(8) :

127   0.15(8) respectively. The CIF files containing details of the structure refinements are available in

128   the Supplemental Files.

129   In the final cycles of refinement, all the atoms in the different structures were refined
130   anisotropically.

131   Details concerning the structure refinement and final results are presented in Table 1 while
132   atomic coordinates, anisotropic displacement parameters and selected bond distances are listed in
133   Tables S1, S2 and S3 of the Supplemental Files.

134

135   **Theoretical calculations**

136   The DFT calculations were performed using the plane-wave pseudopotential method
137   implemented in the Cambridge Sequential Total Energy Package (CASTEP) code (Clark et al.,
138   2005) of the Material Studio program from Accelrys (Materials Studio CASTEP, 2010). The
139   GGA-PBE functional (Hammer, Hansen & Nørskov, 1999) was used to model the exchange and
140   correlation interactions. The Broyden–Fletcher–Goldfrab–Shanno (BFGS) method was used to
141   carry out the geometrical optimization (Shanno, 1985). The plane-wave cut-off energy was
142   adopted to be 500 eV and the Monkhorst–Pack scheme (Perdew, Burke & Ernzerhof, 1996), k-
143   point grid sampling was set to 7x1x1 in the Brillouin zone. As far as self-consistent condition
144   setting is concerned, the total energy was less than 3.10^{-2} eV atom, and the maximum
145   displacement and maximum stress allowed was 10^{-3} Å and 5.10^{-2} GPa respectively. The valence
146   electronic configurations considered for atomic pseudopotential calculation are Nb: $4s^2$ $4p^6$ $4d^4$
147   $5s^1$ and Se: $4s^2$ $4p^4$.

148   To investigate the relative stability of the Nb-SI in the 2H and 3R polytype with an excess of
149   niobium (x = 0.1), 5x1x1 and 5x2x1 supercells respectively are adopted, corresponding to the
150   ordered configurations $Nb_{10}Se_{20}$ (x = 0) and $Nb_{11}Se_{20}$ (x = 0.1) to simulate both pure and SI
151   systems.

152   The formation enthalpy ΔE at T = 0 K is expressed as the difference in total energy of the
153   supercell calculated by DFT and the chemical potentials E of Nb (cubic Fm-3m) and Se (trigonal
154   $P3_121$) calculated from their respective bulks in the same computation conditions.

155

156   $$\Delta E = \frac{1}{(x+y)} [E_{DFT} - xE_{Nb} - yE_{Se}]$$

157

158   where x and y, respectively represent the Nb and Se atoms number in the supercell structure
159   model.

160 The calculated free energy ΔG at typical synthesis temperatures of 760 and 1050 °C only

161 include configurational entropy due to intercalation, according to Ivanova et al., 2019.

162

Results and Discussion

164

X-ray experimental crystal structure

166 The polytype 2H-$Nb_{1.031}Se_2$ is almost stoichiometric (Fig. 1A). Additional metal Nb2 atoms with

167 a refined occupancy about 7.3% are located into the octahedral sites within the van der Waals

168 VDW gap with the stacking sequence AcAδBcB (A,B refer to the selenide layers; c to the

169 completely filled niobium layers and δ to the partially filled niobium layers).

170 Polyhedrons around the Nb atoms are not distorted with six equivalent Nb-Se distances. The

171 Nb1- 6Se = 2.597(2) Å around Nb1 (in a trigonal prismatic coordination) are somewhat larger

172 than the Nb2-6Se = 2.477(2) Å, observed around Nb2.

173 A characteristic feature of this 2H- structure is the short Nb1-Nb2 = 3.1425(6) Å distance,

174 suggesting the formation of strong metal-metal repulsions between the adjacent layers, but can

175 also be analyzed in terms of electrostatic repulsion (Fig. 2A).

176 The relaxation probably occurs following a defect model by introducing vacancy (about 4%) in

177 the Nb1 filled layers. The Nb1 atoms are then displaced forward the created vacancy to minimize

178 the formation of Nb1-Nb2 pairs interactions (Tronc & Moret, 1981; Amzallag et al., 2007).

179 The composition obtained with the structure refinement is : $2H$-($Nb_{0.96(2)} \Delta_{0.04}$) $Nb_{0.073(13)}Se_2$

180 (Δ denotes Nb vacancy in the fully layers) (ie) $2H$-$Nb_{1.031}Se_2$.

181   The Nb1-Se distances in the $3R$-$Nb_{1.071}Se_2$ polytype are very comparable [2.594(9) – 2.601(8)

182 Å] and close to the values [2.59(8) – 2.62(8) Å] reported by Brown & Beerntsen (1965). The

183 refined occupancy (sof) of the additional Nb2 atoms (7.1 %) is almost equal to that observed in

184 the previous 2H structure with the stacking sequence AbAδBcBαCaCβ (A,B,C refer to the

185 selenide layers; a,b,c to the completely filled niobium layers and α,β,δ to the partially filled

186 niobium layers).

187 The octahedrons $Nb2Se_6$ are slightly distorted with three short [2.288(10) Å] and three long

188 [2.698(14) Å] distances. The Nb2 atoms are then shifted from the center of the octahedrons in

189 order to minimize the Nb1-Nb2 [3.425(17) Å] interactions.

190 In order to avoid the direct stacking Nb1—Nb2—Nb1, a relaxation occurs following the

191 transition 2H-3R model and consequently the Nb1-Nb2 distance increases to 3.425(17) Å.

192 Indeed, in the 2H structure the relaxation by introducing high concentration of vacancy in the

193 filled Nb layers may destabilize the structure by breaking the Nb-Nb bonding across the face

194 sharing polyhedrons.

195 In the $3R$-$Nb_{1.085}Se_2$ (Fig. 1B), the refinement reveals a high occupancy, about 11.8%, of

196 additional Nb2 atoms. By comparing with the previous 3R structure, the $Nb2Se_6$ octahedrons are

197 less distorted Nb2-Se = 2.362(11)-2.621(14) Å and the Nb1-Nb2 distance (3.36(2) Å) becomes

198 shorter (Fig. 2B). This can be explained by a shrink of the Nb-Nb layers with high content of

199 extra Nb2 atoms.

200 In this case, both models exhibit relaxation: 2H-3R transition followed by a defect model

201 introducing about 3% of vacancy in the Nb filled layers. A comparable defect was observed in

202 the $3R$-$Nb_{1.06}S_2$ (Powell & Jacobson, 1981).

203 The composition obtained with the structure refinement is : $3R$-$(Nb_{0.97(2)} \Delta_{0.03})$ $Nb_{0.118(13)}Se2$ (Δ

204 denotes Nb vacancy in the fully layers) (ie) $3R$-$Nb_{1.085}Se_2$.

205 In $Nb_{1+x}Se_2$, as in the layered transition metal dichalcogenides, vacancies in the sublattice of

206 the metal (Nb) and chalcogen (Se) are expected.

207 it is quite clear that the increase in the additional Nb induces changes in the pressure of saturated

208 Se vapor above the surface of the growing crystal, and then affects the concentration of selenium

209 vacancies. However, a free refinement of the occupancy of Se atoms in the three polytypes leads

210 to a fully occupied sites, possibly due to the excess of Se used as starting material. Therefore, the

211 generation of vacancies in the sublattice of Nb should be correlated to the location of Nb

212 interlayer.

213 By the presence of extra Nb atoms, a significant residual electron densities are observed in the

214 crystal structure refinements stacking in a way that violates the ideal 2H (ABAB..) and 3R

215 (ABCABC..), about 7.3% for the former and 7.1-11.8% for the latter. The remaining 92.7% and

216 92.9-88.2% are unfaulted (see CIFs in Electronic Supplemental Files). Certainly, a stacking fault

217 is a common feature in this kind of layered structures, with strong diffuse scattering observed

218 along the c^* axis in electron diffraction patterns (see Fig. S1).

219 An indication about the relative stability of 2H and $3R$-$Nb_{1+x}Se_2$ structures, can be obtained

220 by comparing the variation of c/a and (c/n)/a ratios with x, where a and c are the unit cell

221 parameters and n the number of layers in the stacking sequence; n = 2 and 3 for 2H and 3R

222 respectively.

223 As shown in Fig. 3, this ratio change is relatively small with the increase of x for both polytypes

224 with a discontinuity at the 2H to 3R transition around x = 0.07. It is assumed that both polytypes

225 may co-exist in the range $0 < x < 0.07$, and above this limit only the form 3R predominates.

226 Comparable results were observed in the study of the non-stoichiometric 2H and $3R-Nb_{1+x}S_2$

227 $(0.07 < x < 0.18)$ by powder diffraction (Fisher & Sienko, 1980). The mechanism involving the

228 2H-3R transition is still unclear, and may be attributed to the phase limit of the non-

229 stoichiometric $Nb_{1+x}Se_2$. The difference in energy between polytypes is small, thus the

230 possibility to obtain a mixture of polytypes by changing the conditions of synthesis cannot be

231 ruled out.

232   The present results are in agreement with earlier studies by Huisman, Kadijk & Jellinek (1970)

233 and Selte, Bjerkelund & Kjekshus (1966). The mixture 2H and 3R polytype were prepared at

234 temperature of 760°C in the range $0.07 < x < 0.118$, yet the 3R phase at x = 0.07 required higher

235 temperature 1050-1100°C. Further experimental and theoretical works are mandatory to

236 determine the x range of 2H-3R transition accurately.

237

238 **Theoretical results**

239 To corroborate the single X-ray conclusions, the stability of four structures: the pure $2H-NbSe_2$

240 and $3R-NbSe_2$, $2H-Nb_{1.1}Se_2$ and $3R-Nb_{1.1}Se_2$ with 10% of extra Nb-SI in the pure 2H and 3R,

241 respectively, have been investigated. The optimized structural parameters of the supercell

242 structures are summarized in Table 2.

243 The calculated c lattice parameters of 2H and $3R-NbSe_2$ are slightly overestimated compared to

244 the experimental values by 5.28 % and 4.38% respectively. This discrepancy is due to the failure

245 of GGA (local and semi-local approximations for the exchange-correlation) in describing the van

246 der Waals interactions.

247 Structural geometrical optimization revealed that additional Nb2 atoms incorporated in 2H and

248 $3R-Nb_{1+x}Se_2$ with x = 0.1, obviously increase the c parameter by 7.61% and 9.73% respectively

249 while the a parameter remains almost constant.

250   The Nb1-Se distance slightly increases in pure 2H and 3R-NbSe$_2$ (2.587 – 2.600 Å and 2.597 –

251   2.600 Å) compared to 2H and 3R-Nb$_{1.1}$Se$_2$ (2.569 – 2.687 Å and 2.592 – 2.697 Å) while the

252   Nb2-Se distances range from 2.564 – 2.759 Å and 2.610 – 2.797 Å respectively.

253   The calculated formation energies at T = 0 K (Table 2) indicate that the four structures

254   polytypes can be thermodynamically stable. However, due to the strong Nb-Nb interactions the

255   Nb (x = 0.1) SI system is found to be the least favorable. The close free energy ΔG values at high

256   temperature suggest that facile phase transition between the two polytypes may occur, as

257   established between Nb$_2$Se$_3$ and Nb$_{1.33}$Se$_2$ polytypes (Ivanova et al., 2019). These results can

258   explain the experimental stability of both 2H and 3R between 0 < x < 0.07, and confirm the

259   hypothesis of a phase transition from 2H to 3R beyond x = 0.1.

260   The band structures and density of states (PDOS) of the foregoing four cases have been

261   presented to study the impact of the Nb-SI on the electronic structure for both 2H and 3R-NbSe$_2$.

262   Figs. 4A and 4B show the band structure of the pure 2H and 3R respectively. The presence of

263   several bands across the Fermi level E$_F$ reveals the metallic nature of the pure polytypes.

264   Partial density of states (PDOS) (see Figs. S2A and S2C), indicates that the major contribution in

265   DOS at E$_F$ comes from the hybridization between the Nb-4d and Se-4p orbitals which is

266   responsible for the covalent Nb-Se bonds.

267   For both 2H and 3R Nb-SI, the number of electronic bands around E$_F$ apparently increases

268   compared to the pure 2H and 3R (Figs. 4C and 4D), and consequently the gap around 2eV in the

269   Conduction Band disappears. Moreover, the PDOS at E$_F$ decreases and upshifts (see Figs. S2B

270   and S2D) compared to the pure polytypes which implies that a large degree of electrons is

271   transferred by Nb extra atoms into these pure polytypes.

272   It is worth noticing, that the PDOS of Nb-4d is rather broad and almost located at the same

273   energy with Se-4p, suggesting strong interactions. These phenomenon have been observed in

274   some doped and intercalated 2H-NbSe$_2$ (Chen et al., 2014; Hongping et al., 2014a, 2014b;

275   Kouarta, Zanat & Belkhir, 2019; Pervin et al., 2020; Xiao-Chen et al., 2020).

276

277

Conclusions

279   In conclusion, the non-stoichiometric polytypes 2H-Nb$_{1.031}$Se$_2$, 3R-Nb$_{1.071}$Se$_2$ and 3R-Nb$_{1.085}$Se$_2$

280   have been successfully synthesized and investigated by single crystal X-ray diffraction.

281   Although the form 3R predominates for values of x greater than 0.07, both 2H and 3R polytypes

282   may co-exist in the range 0< x <0.07. A transition 2H to 3R polytypes, followed by model

283   vacancies in the host Nb sublattice should take place in order to minimize the Nb_{layer}—Nb_{extra}—

284   Nb_{layer} repulsions between these adjacent slabs.

285   The calculated formation energies of 2H and 3R-$Nb_{1+x}Se_2$ (x = 0, 0.1) by DFT, indicate that both

286   pure and Nb-SI systems can be thermodynamically stable, and suggest an easy phase transition

287   between polytypes. The theoretical outcomes reveal the metallic nature of these polytypes with

288   an overwhelming number of electrons transferred by Nb extra atoms into pure polytypes.

289   Further work involving experimental and theoretical investigations on the Nb-Se system is

290   needed to elucidate the 2H-3R transition mechanism.

291

292

293 **References**

294   Amzallag E, Baraille I, Martinez H, Réat M, Loudet M, Gonbeau D (2007) Electronic and

295   structural properties of Ti vacancies on the (001) surface of TiS_2: theoretical scanning tunneling

296   microscopy images. J Chem Phys 127: 074703– 074703 DOI 10.1063/1.2483592.

297   Brown BE (1966) The crystal structures of WTe_2 and Hight-temperature $MoTe_2$. Acta Cryst

298   20: 268-274 DOI 10.1107/S0365110X66000513.

299   Brown BE, Beerntsen DJ (1965) Layer structure polytypism among niobium and tantalum

300   selenides. Acta Cryst 18:31–36 DOI 10.1107/S0365110X65000063.

301   Bruker (2006). *APEX2*, SAINT, Bruker AXS Inc., Madison, Wisconsin, USA

302   Chen L, Changsheng L, Tang H, Hongping L, Xiaojuan L, Meng J (2014) First-principles

303   calculations on structural, electronic properties of V-doped 2H-$NbSe_2$. RSC Adv 4:9573-9578

304   DOI 10.1039/C3RA47237J.

305   Clark AJ, Segall MD, Pickard CJ, Hasnip PJ, Probert MI, Refson K, Payne MC (2005) First

306   principles methods using CASTEP. Z Krist Cryst Mater 220:22567–22570

307   DOI 10.1542/zkri.220.5.567.65075.

308   Fisher WG, Sienko MJ (1980) Stoichiometry, structure, and physical properties of sulfide. Inorg

309   Chem 19:39–43 DOI 10.1021/ic50203a009.

310 Hammer B, Hansen LB, Nørskov JK (1999) improved adsorption energetic within density-
311 functional theory using revised Perdew-Burke-Ernzerhof functionals. Phys Rev B59:7413–7421
312 DOI 10.1103/PhysRevB.59.7413.

313 Hongping L, Chen L, Zhang K, Liang J, Tang H, Changsheng L, Xiaojuan L, Meng J,
314 Zhongchang W (2014b) Atomic structure and electronic properties of 2H-NbSe$_2$: the impact of
315 Ti doping. J Appl Phys 116:103709-5 DOI 10.1063/1.4895489.

316 Hongping L, Shuai L, Chen L, Wu J, Zhang P, Tang H, Changsheng L, Xiaojuan Li,
317 Zhongchang W, Meng J (2014a) Atomic structures and electronic properties of Ta-doped 2H-
318 NbSe$_2$. RSC Adv 4:57541-57546 DOI 10.1039/C4RA06874B.

319 Huisman R, Jellinek F (1969) On the polymorphism of tantalum diselenide. J Less-Common
320 Metals 17:111-117 DOI 10.1016/0022-5088(69)90041-1.

321 Huisman R, Kadijk F, Jellinek F (1970) The non-stoichiometric phases Nb$_{1+x}$Se$_2$ and
322 Ta$_{1+x}$Se$_2$. J Less-Common Metals 21:187–193 DOI 10.1016/0022-5088(70)90117-7.

323 Ikeura K, Sakai H, Bahramy MS, Ishiwata S (2015) Rich structural phase diagram and
324 thermoelectric properties of layered tellurides Mo$_{1-x}$Nb$_x$Te$_2$. APL Materials 3: 041514-9
325 DOI 10.1063/1.4913967.

326 Ivanova MN, Enyashin AN, Grayfera ED, Fedorov VE (2019) Theoretical and experimental
327 comparative study of the stability and phase transformations of sesquichalcogenides M$_2$Q$_3$ (M =
328 Nb, Mo; Q = S, Se). Phys Chem Chem Phys 21:1454– 1463 DOI 10.1039/C8CP07150K.

329 Kalikhman VL, Umanskii, YaS (1973) Transition-metal chalcogenides with layerstructures and
330 features of the filling of their brillouin zones. Sov Phys Usp 15:728–741
331 DOI: 10.1070/PU1973v015n06ABEH005061.

332 Katzke H (2002) Stacking disorder in 2H-NbS$_2$ and its intercalation. K$_x$(H$_2$O)$_Y$NbS$_2$ I.
333 Description and model calculations of stacking faults in the host lattice NbS$_2$. Z Kristallogr Cryst
334 Mater 217:127–130 DOI 10.1524/zkri.217.4.149.20643.

335 Kouarta H, Zanat K, Belkhir H (2019) Magnetic behavior of superconductor 2H-NbSe$_2$
336 intercalated with iron: first principle study. J Supercond Nov Magn 32:805–819
337 DOI 10.1007/s10948-018-4742-4.

338 Legendre JJ, Moret R, Tronc E, Huber M (1983) Ti$_{1+X}$S$_2$polytypes. Prog. Cryst. Growth
339 Charact. Mater 7:309-342 DOI 10.1016/0146-3535(83)90035-7.

340 Leroux M, Cario L, Bosak A, Rodière P (2018) Traces of charge density waves in NbS_2. Phys
341   Rev B97:195140–195146 DOI 10.1103/PhysRevB.97.195140.

342   Luo H, Xie W, Tao J, Inoue H, Gyenis A, Krizan JW, Yazdani A , Zhu Y, Cava RJ (2015)
343   Polytypism, polymorphism, and superconductivity in $TaSe_{2-x}Te_x$. PNAS 112: E1174-E1180
344   DOI 10.1073/pnas.1502460112.

345   Materials Studio CASTEP Manual © Accelrys, (2010) http://www.tcm.phy.cam.ac.uk/
346   castep/documentation/WebHelp/CASTEP.html

347   Meerschaut A, Deudon C (2001) Crystal structure studies of the $3R-Nb_{1.09}S_2$ and the $2H-NbSe_2$
348   compounds: correlation between nonstoichiometry and stacking type (= polytypism). MRS Bull
349   36:1721–1727 DOI 10.1016/S0025-5408(01)00646-8.

350   Pervin R, Ghosh A, Ghosh H, Shirage PM (2020) Study of transport properties in Se-deficient
351   and Fe-intercalated $NbSe_2$ single crystals: experiment and theory. Mater Sci 55:250–262
352   DOI 10.1007/s10853-019-04002-9.

353 Petříček, V., Dušék, M. & Palatinus, L. (2006) The crystallographic computing system. *JANA*,
354   2006 Institute of Physics, Praha, Czech Republic

355   Powell DR, Jacobson RAJ (1981) The crystal structure of $3-R$ $Nb_{1.06}S_2$. J. Solid State Chem
356   37:140–143 DOI 10.1016/0022-4596(81)90078-5.

357   Predel B (1997). Nb-Se (Niobium-Selenium): Datasheet from Landolt-Börnstein – Group IV
358   Physical Chemistry Volume 5H: Li-Mg – Nd-Zr in Springer Materials DOI 10.1007/b58857.

359   Perdew JP, Burke K, Ernzerhof M (1996) Generalized gradient approximation made simple.
360   Phys Rev Lett 77:3865–3868 DOI 10.1103/PhysRevLett.77.3865.

361 Selte K*, Bjerkelund E, *Kjekshus* A (1966) Intermediate phases in the systems niobium-selenium,
362   niobium-tellurium, tantalum-selenium and tantalum-tellurium. J Less Common Metals 11:14-30
363   DOI 10.1016/0022-5088(66)90053-1.

364   Shanno DF (1985) An example of numerical nonconvergence of a variable-metric   method. J
365   Optim Theory Appl 46:87–94 DOI 10.1007/BF00938762.

366   Sheldrick, G. M. (2002) Program for the refinement of crystal structures. SADABS, Bruker AXS
367   Inc., Madison, Wisconsin, USA

368   Tronc E, Huber M (1973) Polytypisme dans le système titane-soufre. J. Phys. Chem. Solids.
369   34:2045-2058 DOI 10.1016/S0022-3697(73)80053-8.

370   Tronc E, Moret R (1981) Structural aspects of metal-metal interactions in the $Ti_{1+x}S_2$ materials. J

371   Solid State Chem 36:97–106 DOI 10.1016/0022-4596(81)90196-1.

372   Vogel E, Robinson J (2015) Two-dimensional layered transition-metal dichalcogenides for

373   versatile properties and applications. MRS Bull 40:558–563 DOI 10.1557/mrs.2015.120.

374   Wilson JA, Disalvo FJ, Mahajan S (1975) Charge-density waves and superlattices in the metallic

375   layered transition metal dichalcogenides. Adv Phys 24: 117-201

376   DOI 10.1080/00018737500101391.

377   Xiao-Chen L, Shuyang Z, Xueping S, Liangzi D, Xiaolong Z, Youcheng H, Yun-Xiao W,

378   Ching-Wu C, Jia L, Jingjie W, Fu-Sheng K, Pulickel MA (2020) Spontaneous self-intercalation

379   of copper atoms into transition metal dichalcogenides. Sci Adv 6: eaay4092 DOI

380   10.1126/sciadv.aay4092.

Selected single crystal data and structure refinement parameters for the 2H-Nb$_{1.031}$Se$_2$, 3R-Nb$_{1.071}$Se$_2$ and 3R-Nb$_{1.085}$Se$_2$ polytypes.

Nb$_{1+x}$Se$_2$ Polytype	2H-Nb$_{1.031}$Se$_2$	3R-Nb$_{1.071}$Se$_2$	3R-Nb$_{1.085}$Se$_2$
Molar mass (g.mol^{-1})	253.7	257.3	258.1
Crystal size (mm^3)	0.36 x 0.16 x 0.05	0.33x 0.31 x 0.015	0.20 x 0.19 x 0.03
Space group, Z	P6$_3$/mmc, 2	R3m, 3	R3m, 3
Unit cell dimensions (Å)	a = 3.4475(3)	a = 3.4512(4)	a = 3.4670(4)
	c = 12.5702(11)	c = 18.827(3)	c = 18.866(2)
c/a	3.646	5.455	5.441
(c/n)/a	1.823	1.818	1.836
Volume (Å^3)	129.38(2)	194.21(4)	196.39(4)
Calculated density (g.cm^{-3})	6.5101	6.5987	6.5442
Absorption coefficient (mm^{-1})	32.515	32.658	32.33
Angular range θ (°)	3.24- 27.48	6.50-39.95	3.24 - 29.86
Index ranges	-3<h<4 ; -4<k<4	-6<h<6 ; -6< k<4	-4<h<4 ; -4<k<4
	-16<l<16	-32<l<33	-25<l<25
Total recorded reflections	1568	1707	947
Independent reflections, Rint	80, 0.0505	547, 0.0498	188, 0.054
Reflections with I > 3σ(I)	75	534	176
T$_{min}$/T$_{max}$	0.2910/0.7456	0.000/0.615	0.368/0.746
Number parameters	9	14	15
R$_1$, wR$_2$ (all)	0.0882/ 0.1033	0.0232/ 0.0271	0.057/ 0.084
Flack parameter			0.15(8)

The optimized structural constants, selected bond lengths, calculated formation energy ΔE (eV) at 0 K and free energy $\Delta G_{1033,1323}$ (eV) at 1033 and 1323 K for both pure and Nb-SI 2H and 3R-NbSe$_2$ respectively.

1 **Table 2** The optimized structural constants, selected bond lengths, calculated formation energy ΔE (eV)

2 at 0 K and free energy $\Delta G_{1033,1323}$ (eV) at 1033 and 1323 K for both pure and Nb-SI 2H and 3R-NbSe$_2$

3 respectively.

Polytype	a , c (Å)	c/a	(c/n)/a	Nb1–Se , Nb2– Se (Å)	δ (Å)	ΔE	$\Delta G_{1033,1323}$
2H-NbSe$_2$	a = 3.463 , c = 13.210	3.814	1.907	2.587-2.600	0.013	- 1.11	
2H-Nb$_{1.1}$Se$_2$	a = 3.470 , c = 13.807	3.979	1.990	2.569-2.687, 2.564-2.579	0.118 , 0.195	- 0.93	-0.96 , -0.97
3R-NbSe$_2$	a = 3.506 , c = 19.708	5.621	1.873	2.597–2.600	0.03	-1.25	
3R-Nb$_{1.1}$Se$_2$	a = 3.412 , c = 21.679	6.300	2.100	2.592–2.697, 2.610–2.797	0.105 , 0.187	- 0.94	-0.97 , -0.98

5 Note: same notation for Nb and Se atoms as used in X-ray refinement tables. The distortion δ (Å) is the

6 difference between the longest and shortest Nb-Se bond distance.

Figure 1

Crystal structure of (A) $2H$-$Nb_{1.031}Se_2$; (B) $3R$-$Nb_{1.085}Se_2$ showing the prismatic packing of $Nb1Se_6$ polyhedron (drawn in blue) and $Nb2Se_6$ (drawn in purple).

The extra Nb2 atoms are located into the octahedral sites ($Nb2Se_6$ drawn in purple) within the van der Waals gap.
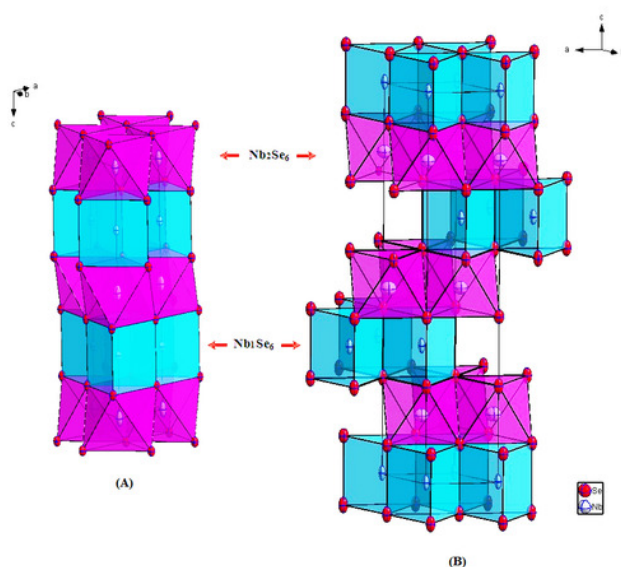
Figure 2

Projection of the crystal structures of (A) $2H$-Nb$_{1.031}$Se$_2$; (B) $3R$-Nb$_{1.085}$Se$_2$ along the [100] direction, showing the Nb_{layer}—Nb_{extra}—Nb_{layer} repulsions (red arrows).

Thermal ellipsoids are drawn at 95% probability displacement level.
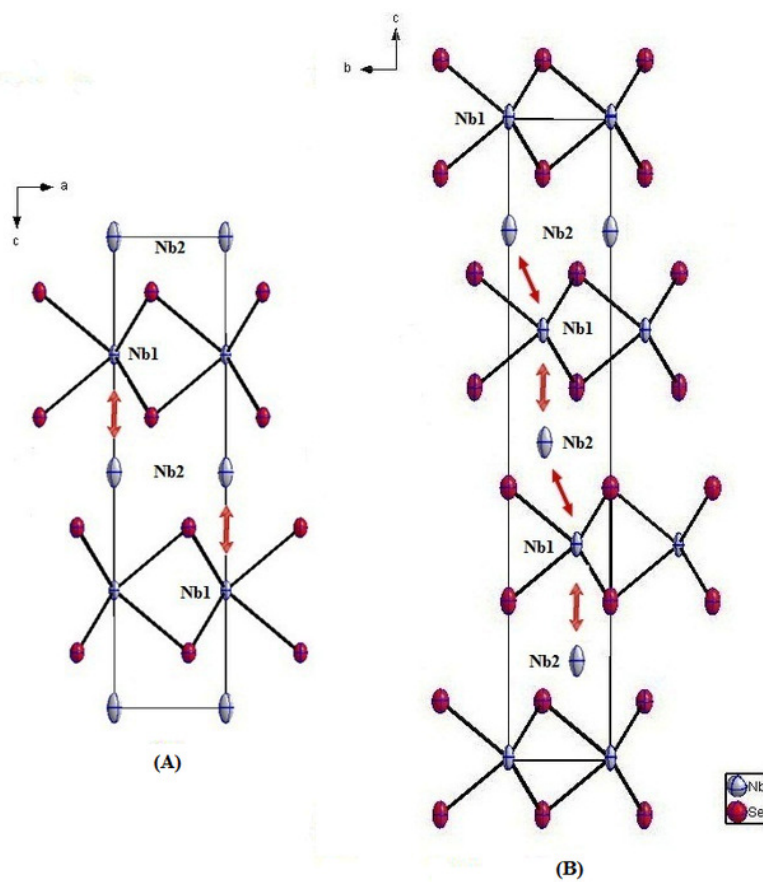
Figure 3

The reduced lattice parameters ratio (A) c/a; (B) (c/n)/a for 2H and 3R-$Nb_{1+x}Se_2$ (0<x<0.1) polytypes.

The values at x=0 for 2H and 3R are calculated respectively from the references (Brown & Beerntsen, 1965) and (Meerschaut & Deudon, 2001).
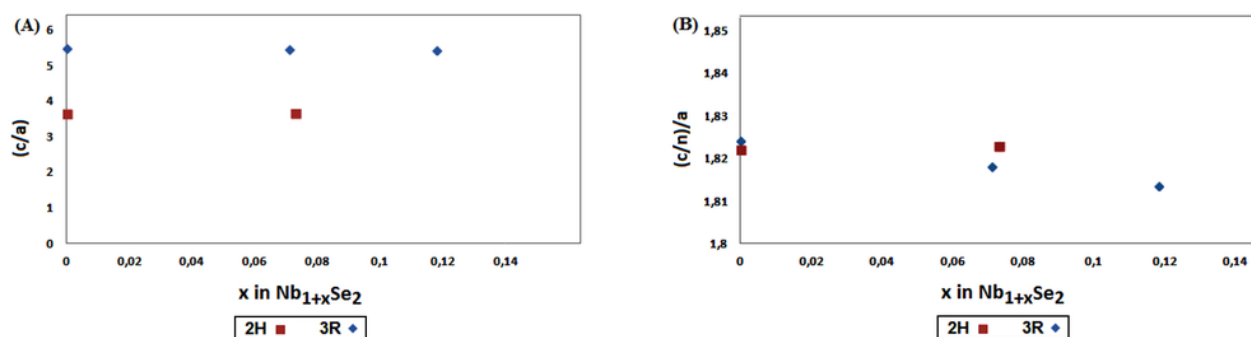
Figure 4

Electronic band structure and their corresponding DOS of (A) 2H-NbSe$_2$; (B) 2H-Nb$_{1.1}$Se$_2$, (C) 3R-NbSe$_2$; (D) 3R-Nb$_{1.1}$Se$_2$.